Precipitation driving of droplet concentration variability in marine low clouds

***Robert Wood[1], David Leon[2], Matthew Lebsock[3], Jefferson Snider[2], Antony D. Clarke[4]**

1. Department of Atmospheric Sciences, 408 ATG Building, University of Washington, Seattle, WA, 98195-1640, USA.

2. Department of Atmospheric Sciences, University of Wyoming, Dept. 3038 1000 E. University Ave., Laramie, WY 82071, USA

3. Jet Propulsion Laboratory, California Institute of Technology, 4800 Oak Grove Drive, Pasadena, California 91109-8099, USA

4. Department of Oceanography, University of Hawai`i at Manoa, 1000 Pope Road, Marine Sciences Building, Honolulu, HI 96822, USA

* Corresponding author (robwood@atmos.washington.edu

Tel: 206-543-1203; Fax: +1 206 685 9302)

Version 4 (March 18th, 2012)

The concentration N_d of cloud droplets in marine low clouds is a primary determinant of their ability to reflect sunlight and modulates their ability to precipitate. Previous studies have focused upon aerosol source variability as the key driver of N_d variability. Here, we show for the first time that a highly simplified aerosol budget model constrained with new satellite measurements of light precipitation and recent field observations of above-cloud aerosol particles, can predict with skill the geographical variability of N_d in regions of extensive marine low clouds. Precipitation is shown to be a major driver of N_d variability in marine stratocumulus. Apart from very close to continental coastlines, where pollution sources are dominant, the model is able to reproduce observed N_d variability by assuming a fixed concentration of free-tropospheric cloud condensation nuclei (CCN) and a wind-speed dependent surface source. Surface CCN sources alone are insufficient to maintain N_d against precipitation losses. The results provide new observational constraints on the factors controlling marine cloud microphysical properties globally and demonstrate that even light precipitation rates typical of marine stratocumulus exert a profound impact upon these clouds.

Anthropogenic activities have resulted in marked increases in the concentration of aerosol particles in the atmosphere[1,2] and these increases exert a significant but highly uncertain radiative forcing on the global climate[2,3]. A large fraction of this forcing is attributed to the effects that aerosol particles have on clouds by increasing the concentration N_d of cloud droplets[4,5,6], reducing droplet size[7], and increasing the reflected

48 solar radiation[8,9,10]. Systematic increases in N_d have been observed downwind of east
49 Asia over the past two decades[11] and have been attributed to rapid industrialization. The
50 magnitude of the so-called "aerosol indirect effect" on climate depends not only upon the
51 present-day conditions, but also upon the unperturbed microphysical state of the clouds
52 prior to adding anthropogenic aerosols[11]. Therefore N_d is the single most important
53 microphysical variable that must be accurately represented in models in order to
54 accurately determine aerosol indirect effects on climate. However, there are marked
55 differences between values of N_d in different climate models[10,12,13] demonstrating a clear
56 lack of understanding of the key controls on N_d.

57 Satellite-based studies use the relationship between observed cloud droplet size or
58 concentration, and nearby clear-sky estimates of aerosol loading, to infer the role that
59 aerosols play in influencing clouds and climate[7]. Some even go so far as to quantitatively
60 estimate aerosol indirect effects globally[14,15]. Inherent in this approach is that correlations
61 between cloud microphysical properties and aerosols in the current climate are indicative
62 of an aerosol influence on cloud properties rather than vice versa. It is a common
63 experience that clouds can impact aerosol particle concentrations under certain
64 circumstances, a commonplace example of which is the buildup of haze during dry
65 periods and its clearing after rain. Aerosol-cloud correlative studies do not take the
66 possible effects of precipitation into account. One can make a reasonable case that
67 precipitation-induced aerosol changes will not significantly impact the inferences drawn
68 from these studies only if one assumes that the impacts of precipitation are localized,
69 intermittent, and relatively rare, and that the aerosol fields that interact with the majority
70 of clouds are not significantly affected by precipitation. However, recent observations

from the sensitive spaceborne radar on the CloudSat satellite are finding that precipitation occurs more frequently over the globe than previously thought[16,17] prompting a re-examination of the role of precipitation in driving aerosol variability.

In this study we use these state-of-the-art quantitative estimates of light precipitation from CloudSat to constrain a simple budget model that predicts the mean concentrations of cloud condensation nuclei (CCN) and cloud droplets over those parts of the global oceans containing extensive low clouds. These clouds are confined within the marine boundary layer (MBL) and are among the most susceptible to aerosol perturbations[12]. We build upon previous studies[18,19] that used simplified budget models to provide important insights into the factors controlling CCN, by constructing a steady-state budget for CCN in the MBL appropriate for the regions of large-scale subsidence where extensive marine stratocumulus clouds are favored[20].

The rate of increase of CCN concentration $\dot{N}$ averaged over the depth of the MBL can be written as the sum of various source and sink terms:

$$\dot{N} = \dot{N}_{\mathrm{FT}} + \dot{N}_{\mathrm{S}} + \dot{N}_{\mathrm{P}} + \dot{N}_{\mathrm{DRY}} + \dot{N}_{\mathrm{ADV}} \quad [1]$$

where $\dot{N}_{\mathrm{FT}}$, $\dot{N}_{\mathrm{S}}$, $\dot{N}_{\mathrm{P}}$, $\dot{N}_{\mathrm{DRY}}$, and $\dot{N}_{\mathrm{ADV}}$ are the time tendencies due to entrainment of CCN from the free-troposphere (FT), primary production at the surface (i.e. sea spray), precipitation (i.e. coalescence scavenging), dry deposition to the surface, and horizontal advection respectively. The model does not take into account CCN formation from the nucleation of new particles in the MBL since it is unlikely that this contributes significantly to the mean CCN number concentration over the oceans. In severely-scavenged ultraclean MBLs evidence of new particle formation has been noted[21,22,23,24]. Such nucleation events appear to be quite rare, with only one clear instance observed

during four weeks of shipborne sampling over the tropical southeastern Pacific ocean[25]. In addition, evidence that freshly nucleated particles can grow to sufficient sizes to increase the population of CCN without being scavenged by existing cloud is lacking. Nucleation events are therefore unlikely to compete with other source processes in determining the mean state[25,26]. In any case, formulations for the rate of production of CCN from new particle formation in the MBL are highly uncertain[27,27].

Free-tropospheric air is constantly being mixed into the MBL by cloud top entrainment, and this can either provide a net source of CCN to the MBL or can dilute MBL aerosol concentrations. Modeling and observational studies suggest that the FT is a primary source of CCN in the remote MBL[22,27,28]. The net source rate $\dot{N}_{FT} = w_e(N_{FT}–N)/z_i$ where z_i is the depth of the MBL and w_e is the entrainment rate. We constrain N_{FT} based on aerosol measurements from field data taken in the Southern and Northern Hemisphere remote subtropical FT. Time-mean CCN concentrations west of 75°W over the southeastern Pacific Ocean (Fig. 1a and Supplementary Fig. 1) are in remarkably good agreement with estimates from a composite time-mean size distribution measured over 17 days with large scale subsidence at a remote FT station on Mauna Loa[29] during July 1992. This is perhaps surprising because although the southeastern Pacific and Hawaii are in similar tropical meteorological regimes, one might expect marked differences in the mean size distribution due to the different array of sources and landmasses in the Northern and Southern Hemisphere. The mean distributions are made up of a mixture of different aerosol populations from a number of different sources. Previous studies[29,30,31] suggest that new particle formation from naturally-produced sulfuric acid in the upper troposphere constitutes one major source of clean FT CCN. This aerosol subsequently

subsides in the descending branches of large scale atmospheric systems where its distribution is expected to reach a quasi-steady state[31,32]. In addition, the remote marine FT also includes air masses transported long distances from continents which likely contain some pollution aerosol. In the model we assume a constant mean concentration N_{FT} = 125 cm^{-3} everywhere, which is within 20% of the time-mean values derived from the remote subtropical data in both hemispheres (see Supplementary Fig. 1), and is consistent with peak supersaturations in marine stratocumulus clouds (see the Methods section).

The modeled surface source $\dot{N}_S$ is assumed to be from primary production of sea-spray aerosol (SSA) and we use a recent parameterization[32] to provide $\dot{N}_S = F(\sigma) U_{10}^{3.41}/z_i$ where U_{10} is the wind speed at a height of 10 m, and $F(\sigma)$ depends upon the assumed peak supersaturation σ experienced in the clouds (see the Methods section).

The precipitation sink term $\dot{N}_P$ depends upon the precipitation rate at cloud base P_{CB}. We use a formulation which accounts for losses from the collection of cloud droplets by precipitation drops in the cloud via accretion[33]. This gives $\dot{N}_P = K\, N\, P_{CB}\, h/z_i$, where K = 2.25 m^2 kg^{-1} is a constant that depends upon the collection efficiency of cloud droplets by drizzle drops[34], and h is the cloud thickness.

Dry deposition $\dot{N}_{DRY}$ is found to be of negligible import over the oceans (see Methods section) and so is ignored. We also ignore the advective term $\dot{N}_{ADV}$ to avoid the complication of calculating spatial gradients and to facilitate the interpretation of the key physical processes controlling N_d (see Methods section).

In this study we examine the time-mean CCN budget by setting $\dot{N}$=0 in equation (1) inserting the expressions discussed above for the various terms, and

rearranging to obtain an expression for the steady-state value N_{eq} of the CCN concentration in the MBL as

$$N_{eq} = \frac{\left(N_{FT} + \frac{F(\sigma)U_{10}^{3.41}}{Dz_i}\right)}{\left(1 + \frac{hKP_{CB}}{Dz_i}\right)} \quad [2]$$

Here we have also assumed that entrainment is in balance with the large-scale subsidence rate, so that $w_e = D\, z_i$,.where D is the large scale divergence, appropriately assumed to be constant with height over the depth of the MBL[34]. In practice, the entrainment rate exceeds the subsidence rate by 10-40% over the subtropical stratocumulus regions[35], but estimating its precise value is itself a major challenge[36] and is not attempted here.

To assess the quality of the model, we use recent field measurements from a major observational program focused on sampling the lower troposphere over the tropical southeastern Pacific Ocean[37]. The measurements sampled the largest semi-permanent subtropical sheet of stratocumulus on Earth that extends westward from the Chilean and Peruvian coasts. Extensive survey sampling was carried out along 20°S from the Chilean coast at 70°W to ~1400 km offshore at 85°W using a combination of different research aircraft. Measurements were made in both the MBL and the lower FT. Figure 1a shows observations of the two key inputs to the budget model, namely the time-mean FT CCN concentration and the precipitation rate close to the cloud base. CCN concentrations in the FT fall off sharply within 500 km of the coast but despite considerable day to day variability, the time-mean campaign values remain relatively constant for over 1000 km

160 out to 85°W (Fig 1a). Several lines of evidence point to anthropogenic pollution being
161 responsible for the high values very close to the coast[38].

162 The cloud base precipitation rate increases markedly with distance from the
163 Chilean coast, from an essentially nonprecipitating state with <0.1 mm d^{-1} near the coast
164 to >1 mm d^{-1} at 85°W (Fig. 1a). Rates of 1 mm d^{-1} are sufficient to drive significant
165 coalescence scavenging of CCN[34,39]. This gradient in precipitation is driven to a
166 significant extent by thickening clouds and a deeper boundary layer to the west[40].
167 Precipitation in marine stratocumulus maximizes at night[17], and is typically heaviest in
168 the early morning hours when the clouds are at their thickest[41]. This is apparent in the
169 observations where precipitation rates are lowest at 1:30pm (CloudSat, daytime
170 overpass), take intermediate values at 1:30am (CloudSat nighttime overpasss) and are
171 largest during 03-09 am (VOCALS field data). Since the timescale for CCN removal due
172 to precipitation is typically > 1 day given these precipitation rates[35], we use a daily mean
173 estimate as the mean of the two CloudSat overpasses to drive the model.

174 In addition to FT CCN and precipitation, we use wind speed and surface
175 divergence estimates from the QuikScat satellite[35], MBL depth and cloud thickness
176 estimates from the MODIS satellite[36]. The model, when forced with CloudSat observed
177 mean precipitation rates and observed FT CCN, captures the observed increase in N_d as
178 the coast is approached (Fig. 1b) with remarkable fidelity given the model's simplicity.
179 The model produces a factor of two increase in N_d from 90°W to 75°W even when the
180 model is forced with a fixed FT CCN concentration of 125 cm^{-3} (consistent with mean
181 values over the remote region away from the coast). With fixed CCN, however, the
182 model is unable to reproduce the highest concentrations within 500 km of the coast.

183 However, these values are obtained with the observed longitudinally-varying FT CCN
184 concentration increase that includes the near-coastal enhancement due to pollution
185 sources[39] (Fig 1b). The general behavior of decreasing N_d from 75-90°W can be
186 explained by increasing precipitation scavenging (Fig. 1a), which can be seen by
187 comparing the model estimates with fixed FT CCN and either no precipitation or
188 precipitation fixed at a constant value of 1 mm d^{-1} (Fig 1b). A critical finding here is that
189 a precipitation rate of as little as 1 mm d^{-1} is sufficient to drive down N_d by a factor of
190 three over the remote ocean, which further serves to emphasize the importance of
191 precipitation in controlling mean cloud droplet concentrations over the remote ocean.
192 Primary production from sea-spray constitutes a weaker, but significant, source than
193 entrainment from the FT consistent with a previous study with the same
194 parameterization[33]. However, it is important to note that we are using a source function
195 that is one of the more prolific available[42], although experimentation with different
196 primary production parameterizations only changes the modeled N_d values by less than
197 20% (see Supplementary Figure 2) and does not affect our conclusions regarding the
198 importance of precipitation.
199 Given the ability of the budget model with fixed FT CCN concentrations to
200 reproduce with some skill the gradient in N_d over the remote southeastern Pacific Ocean,
201 we apply the model more generally to regions of extensive marine low cloud under
202 conditions of large scale subsidence (Fig. 2). Aerosol concentrations in the FT vary
203 significantly both regionally and in response to variations in natural and anthropogenic
204 sources[43]. Because there are no global observational constraints on the time-mean FT
205 CCN, we draw on the consistency between mean FT CCN spectra at Mauna Loa and over

206 the southeastern Pacific Ocean (Fig. 1) and fix N_{FT} = 125 cm^{-3} everywhere for the base
207 case (see Methods section). The satellite observations show that cloud droplet
208 concentrations N_d in excess of 150 cm^{-3} tend to be located near the continental coastlines
209 (e.g. California, Chile/Peru, Europe), with values reducing toward the remote oceans,
210 where they are as low as 20-60 cm^{-3}. The base case is able to reproduce well the mean
211 values (Table 1) and geographical variability in N_d (Fig. 2) for low cloud regions,
212 especially for the remote subtropical/tropical regions 35°S-35°N. The model
213 underestimates N_d close to coastlines (Table 1) consistent with a lack of continental
214 sources. The model also captures the low values (<60 cm^{-3}) over the remote North Pacific
215 and Atlantic and the Southern Ocean north of 45°S. Removing the precipitation sink
216 increases mean N_d in the model by a factor of 2-3 over the remote oceans, but only 15%
217 in the near-coastal regions where precipitation rates are very low (Table 1). A doubling of
218 N_{FT} from 80 to 160 cm^{-3} leads to a 50-70% increase in N_d (Table 1) because FT CCN is
219 partly buffered by surface sources.
220 The skill in predicting N_d is remarkable given that there is no variation
221 whatsoever in the FT CCN source in Fig. 2. To examine the key factors controlling the
222 geographical variability of N_d in the model, we conduct additional model sensitivity
223 experiments. In each experiment, only one of the variables in equation (2) is allowed to
224 vary. All other variables are fixed by setting them to their respective mean values over
225 time and space (Table 2). It is clear that precipitation variability is required in order to
226 produce the strong correlation with observations seen in the base case (r = 0.65). No
227 other variable can alone explain more than 15% of the observed geographical variance in
228 N_d. Divergence and cloud thickness variations also lead to model fields with significant

positive correlations (r =0.21 and 0.37 respectively), but the geographical variability in N_d driven by these variables is far too weak to explain the observed variability (Table 2). The correlations are positive because divergence and cloud thickness correlate quite well with precipitation itself. We find that wind speed variability alone explains an insignificant amount of the model N_d variability (r = -0.06), from which we conclude that variability in SSA is not a significant contributor to the observed N_d variability. This is especially true in the subtropics and tropics where wind speeds are relatively modest and the FT source is greater than the surface source (Supplementary Fig. 3). However, SSA does contribute to the mean N_d (Table 1) despite not substantially impacting its geographical variance.

Overall, these results lead us to argue that a large fraction of the observed geographical variability in cloud droplet concentration in extensive marine low clouds over the remote oceans is driven by precipitation losses rather than aerosol source variability. This is further demonstrated by noting the striking similarities between the maps of the mean observed precipitation rates from low clouds (Fig. 3) and the observed N_d field (Fig. 2).

Frequency distributions of monthly mean N_d (Fig. 4) show that the base case model (N_{FT} = 125 cm^{-3}) can represent satellite-observed N_d variability well. As we might expect from Fig. 2, the model is unable to capture the very highest concentrations observed by the satellite (N_d > 200 cm^{-3}) that are mostly regions within a few hundred kilometers of coastlines. This is because neither the advection of continentally-influenced MBL air nor elevated near-coastal FT concentrations (e.g., Fig. 1) are considered in the model. When the model is forced by removing either FT CCN or SSA production, the

model is unable to represent the distribution of observed N_d and underestimates the mean N_d (see also Table 1). This further emphasizes that the surface and FT are both important contributors to the cloud droplet concentration over the remote oceans[29,32,33]. The shape of the model N_d distribution is relatively insensitive to plausible variations in the assumed FT CCN concentration (Supplementary Fig. 4).

Our results have a number of important implications. First, if CCN and cloud droplet concentration variability over much of the global ocean are determined by precipitation variability rather than aerosol source variability, this calls into question the interpretation of correlative studies[15,16] linking cloud properties to aerosol properties as providing useful information on anthropogenic aerosol indirect effects on climate. It also suggests that the notion of there being a 'background' aerosol concentration in the unperturbed marine boundary layer may not be a useful one because MBL CCN concentrations are strongly modulated by precipitation processes that vary strongly both geographically and temporally. The FT CCN over remote oceanic regions is known to reflect a complex mixture of different sources, some of which are natural and some anthropogenic. Our finding that a relatively constant time-mean FT CCN supply appears to be sufficient to explain much of the mean gradients in the cloud droplet concentration over the remote oceans should not therefore be interpreted as indicating that the remote oceanic regions are devoid of anthropogenic influence. The increasing concentrations observed within about 500 km of continents most likely reflects a lower tropospheric pathway for continental aerosols, whereas the more remote anthropogenic contributions are associated with aerosol or precursors lofted higher into the troposphere that can then be transported long distances before subsidence carries them into the MBL.

Here we have shown that MBL cloud droplet concentrations are impacted by precipitation, but we note that an increasing body of evidence shows that precipitation in low clouds typically decreases with cloud droplet concentration[44]. There is then the potential for a significant positive feedback whereby modest increases in CCN reduce the precipitation sink, amplifying the initial perturbation. Although we do not claim evidence for bistability in the system[19], our results do suggest that pollution-driven CCN increases may be amplified by precipitation suppression and that this warrants further exploration with more sophisticated models.

Finally, we note that climate models tend to impose fixed limits on cloud droplet concentration minima[10] suggesting deficiencies in modeling the processes responsible for low concentrations over the remote ocean. A closer focus on the role of precipitation is now needed to better understand whether climate models are able to produce light precipitation in the marine boundary layer, and whether the models are impacted appropriately by it. This study helps to highlight that we now have the satellite measurements of light precipitation and cloud microphysical properties to begin to explore this critical control on cloud microphysical properties.

Methods

The CCN budget model (equations 1 and 2) implicitly assumes that the cloud droplet concentration N_d and the CCN concentration are one and the same. This is reasonable provided that (a) we choose an appropriate peak supersaturation σ in order to convert the aerosol sources, which are provided as a function of aerosol size, into tendencies of CCN; (b) the cloud droplet concentration throughout the cloud is equal to that determined by the aerosol activation process. For marine stratocumulus clouds, observations suggest that values of σ in the range 0.1-0.8% are typical with mean values around 0.3% consistent with observations[4,45]. Here we assume a constant value of σ=0.3% for all calculations. While this does not account for variability in supersaturation driven by changes in the strength of turbulence and changes in CCN concentration, we provide some justification (Supplementary Fig. 1) that systematic changes in supersaturation over the remote oceans are relatively small.

We derive a value of N_{FT} in the range 100-175 cm^{-3} active at σ=0.3% from the mean size distribution (assuming a plausible range of aerosol hygroscopicity, see Supplementary Fig. 1) obtained during subsiding conditions at a FT site in Hawaii[30]. This which is in remarkable agreement with mean values from CCN spectrum measurements made in the southern hemisphere subtropical FT during the VOCALS Regional Experiment (see Fig. 1a).

For the surface source, we use a size-resolved sea spray generation function[33] to estimate the rate of particle generation for particles active at σ=0.3% supersaturation. This yields $F(\sigma)$= 214 m^{-3} $(m\,s^{-1})^{-2.41}$. For a wind speed of 8 m s^{-1} this yields $\dot{N}_S$ = 22 cm^{-3} d^{-1} averaged over an MBL that is 1 km deep. The widely-used source

function of Monahan (see Supplementary Fig. 2) has the same wind speed dependence but a rate which is over a factor of two lower.

Dry deposition of CCN to the ocean is estimated using deposition velocity parameterization[46] for accumulation mode particles (0.05-1 μm diameter) which make up the bulk of the CCN in the MBL. Rates are in the range 0.001-0.01 cm s^{-1} with the higher values occurring at higher wind speeds and for the larger of the accumulation mode particles. Given these deposition velocities, we find that dry deposition constitutes only a very weak sink for CCN under most circumstances, with loss rates unlikely to exceed 2 cm^{-3} d^{-1} for most values of N observed, and most wind speeds, over the oceans.

The magnitude of the advection term $\dot{N}_{\mathrm{ADV}}$ can be estimated using the observed cloud droplet concentration from satellite[47]. Over the remote oceans the magnitude of $\dot{N}_{\mathrm{ADV}}$ is generally 10 cm^{-3} d^{-1} or less, while higher values can be found in near-coastal regions. Including advection in the steady state model introduces an additional level of complexity since it involves taking spatial gradients. To preserve simplicity we omit it from the model. Since precipitation is the dominant control on N_{d} in the model, the geographic pattern of the advection term largely follows the spatial gradient in precipitation rate.

Model estimates are produced globally on a 1×1° grid on a month by month basis. Cloud droplet concentration estimates from the Moderate Resolution Imaging Spectroradiometer (MODIS) on the NASA Terra satellite are produced from daily Level 3 data for 1x1° boxes using a visible/near infrared approach[48]. To minimize problems of retrievals in broken clouds, we only include in our averages those daily boxes where the cloud cover from liquid clouds exceeds 0.8. These are then averaged

340 together to provide monthly mean N_d estimates. Annual means are estimated from only
341 those months with positive mean surface divergence, mean cloud top height lower than
342 4 km, and with mean liquid cloud fractions exceeding 0.3. Annual mean data are only
343 analyzed for those locations where at least four months pass the acceptance criteria.

344 The model is driven by new precipitation rate estimates from a profiling W-band
345 radar on the CloudSat satellite[49]. The cloud base precipitation rate needed to calculate the
346 coalescence scavenging[34] is estimated as the maximum value in each radar profile. Mean
347 precipitation rates from low clouds are estimated for 5×5° gridboxes globally by
348 removing profiles with detectable echoes above the 3 km level. For the regions
349 considered, the results are not strongly sensitive to the choice of this level since the
350 majority of the clouds are situated below 2 km. Gridded precipitation rates are produced
351 on a monthly basis for data from 2006-2009.

352 To drive SSA production we use daily mean wind speed estimates from the
353 QuikScat satellite and average the production rates up to monthly averages. Including
354 sub-daily timescale variability in wind speed increases the surface production of SSA, but
355 we find from reanalysis data that including 6 hourly estimates increases SSA production
356 by less than 10%. Boundary layer depth z_i is estimated using from MODIS cloud top
357 temperature retrievals[36], and cloud thickness h is estimated with an adiabatic assumption
358 using MODIS retrievals of cloud liquid water path[36]. Both are taken from 1×1° gridded
359 daily Level 3 MODIS products.

360
361
362
363
364
365

366
367
368
369

370

371 **References**
372

[1] Kaufman, Y., D. Tanré, and O. Boucher. A satellite view of aerosols in the climate system. *Nature*, **419**, 215-223 (2002).

[2] Isaksen, I. S. A. et al. Atmospheric composition change: Climate–Chemistry interactions. *Atmospheric Environment*, **43**, 5138-5192 (2009).

[3] IPCC, 2007. Climate Change: The Physical Science Basis. Contribution of Working Group I to the Fourth Assessment Report of the Intergovernmental Panel on Climate Change. S. Solomon, D. Qin, M. Manning, Z. Chen, M. Marquis, K.B. Averyt, M.Tignor and H.L. Miller (eds.) Cambridge University Press, Cambridge, United Kingdom and New York, NY, USA (2007).

[4] Martin, G. M., D. W. Johnson, and A. Spice. The measurement and parameterization of effective radius of droplets in warm stratocumulus clouds. *J. Atmos. Sci.*, 51, 1823–1842 (2004).

[5] Ramanathan, V., P. J. Crutzen, J. T. Kiehl, and D. Rosenfeld. Aerosols, climate, and the hydrological cycle. *Science*. **294**, 2119-2124 (2001).

[6] Lohmann, U., and J. Feichter. Global indirect aerosol effects: a review. *Atmos. Chem. Phys. Disc.* 5, 715–737 (2005).

[7] Bréon, F. M., Tanre, D., Generoso, S. Aerosol effect on cloud droplet size monitored from satellite. *Science*, **295,** 834-838 (2002).

[8] Twomey, S., 1974: Pollution and the planetary albedo. *Atmos. Env.,* 8, 1251–1256.

[9] Penner, J. E., X. Q. Dong, and Y. Chen. Observational evidence of a change in radiative forcing due to the indirect aerosol effect. *Nature*., **427**, 231-234 (2004).

[10] Quaas, J et al. Aerosol indirect effects – general circulation model intercomparison and evaluation with satellite data, *Atmos. Chem. Phys*., **9**, 8697-8717 (2009).

[11]Bennartz, R., J. Fan, J. Rausch, L. R. Leung, and A. K. Heidinger. Pollution from China increases cloud droplet number, suppresses rain over the East China Sea, Geophys. Res. Lett., 38, L09704, doi:10.1029/2011GL047235 (2011).

[11] Oreopoulos L., and S. Platnick. The radiative susceptibility of cloudy atmospheres to droplet number perturbations: 2. Global analysis from MODIS *J. Geophys. Res.*, **113**, D14S21 (2008).

[12] Ming, Y, V. Ramaswamy, L. J Donner, and V. T. J. Phillips. A new parameterization of cloud droplet activation applicable to general circulation models. *J. Atmos. Sci..*, **63**, DOI:10.1175/JAS3686.1 (2006).

[13] Gettelman, A., H. Morrison, S. J. Ghan. A New Two-Moment Bulk Stratiform Cloud Microphysics Scheme in the Community Atmosphere Model, Version 3 (CAM3). Part II: Single-Column and Global Results. *J. Climate*, **21**, 3660–3679 (2008).

[14] Quaas, J., O. Boucher, N. Bellouin, and S. Kinne. Satellite-based estimate of the direct and indirect aerosol climate forcing, *J. Geophys. Res.*, 113, D05204, doi:10.1029/2007JD008962 (2008).

[15] Jones, T. A., Christopher, S. A., and Quaas, J. A six year satellite-based assessment of the regional variations in aerosol indirect effects, *Atmos. Chem. Phys.*, **9**, 4091-4114, (2009)

[16] Leon, D. C., Z. Wang, and D. Liu. Climatology of drizzle in marine boundary layer clouds based on 1 year of data from CloudSat and Cloud-Aerosol Lidar and Infrared Pathfinder Satellite Observations (CALIPSO), J. Geophys. Res., 113, D00A14 (2008).

[17] Haynes, J. M., T. S. L'Ecuyer, G. L. Stephens, S. D. Miller, C. Mitrescu, N. B. Wood, and S. Tanelli. Rainfall retrieval over the ocean with spaceborne W-band radar, J. Geophys. Res., 114, D00A22, (2009).

[18] Baker, M. B., and R. L. Charlson. Bistability of CCN concentrations and thermodynamics in the cloud-topped boundary layer. *Nature*, **345,** 142–145 (1990).

[19] Baker, M. B. Variability in concentrations of cloud condensation nuclei in the marine cloud-topped boundary layer. *Tellus*, **45B,** 458–472 (1993).

[20] Klein, S. A. and D. L. Hartmann. The seasonal cycle of low stratiform clouds. *J. Climate*,, 6, 1588–1606 (1993).

[21] Clarke, A. D., et al., Particle nucleation in the tropical boundary layer and its coupling to marine sulfur sources, Science, 282, 89– 92 (1998).

[22] Petters, M. D., J. R. Snider, B. Stevens, G. Vali, I. Faloona, and L. M. Russell (2006), Accumulation mode aerosol, pockets of open cells, and particle nucleation in the remote subtropical Pacific marine boundary layer, J. Geophys. Res., 111, D02206, doi:10.1029/2004JD005694.

[23] Tomlinson, J. M., R. Li, and D. R. Collins. Physical and chemical properties of the aerosol within the southeastern Pacific marine boundary layer, J. Geophys. Res., 112, D12211 (2007).

[24] Wood, R., K. K. Comstock, C. S. Bretherton, C. Cornish, J. Tomlinson, D. R. Collins, and C. Fairall. Open cellular structure in marine stratocumulus sheets, *J. Geophys. Res.*, 113, D12207 (2008).

[25] Capaldo K. P., Kasibhatla P., and Pandis S.N. Is aerosol production within the remote marine boundary layer sufficient to maintain observed concentrations? *J. Geophys. Res.*,**104**, 3483-3500 (1999).

[26] Katoshevski, D., Nenes, A., and Seinfeld, J. H. A Study of processes that govern the maintenance of aerosols in the marine boundary layer, *J. Aerosol Sci.*, **30**, 503-532 (1999).

[27] Kirkby, J., et al., Role of sulphuric acid, ammonia and galactic cosmic rays in atmospheric aerosol nucleation. *Nature*, **476**, 429-433 (2011).

[28] Clarke, A. D., J. L. Varner, F. Eisele, R. L. Mauldin, D. Tanner, and M. Litchy. Particle production in the remote marine atmosphere: Cloud outflow and subsidence during ACE 1, *J. Geophys. Res.*, 103(D13), 16,397–16,409 (1998).

[29] Weber, R. J. and P. H. McMurry. Fine particle size distribution measurements at Mauna Loa Observatory, Hawaii, *J. Geophys. Res*., **101**, 14767-14775 (1996).
Long term measurements in the free troposphere at Mauna Loa show an annual cycle in submicron aerosol light scattering of about a factor of three with a maximum in Spring largely in response to dust and pollution transport from Asia, and a minimum in Autumn. Conditions in July, when the detailed size distribution measurements were made, lie between the maximum and minimum values and we consider them broadly representative of the annual mean conditions at the site.

[30] Friedlander, S.K. *Smoke, dust and haze*. John Wiley and Sons (1977).

[31] Raes, F. Entrainment of free tropospheric aerosols as a regulating mechanism for cloud condensation nuclei in the remote marine boundary layer, *J. Geophys. Res.*, **100**, 2893–2903 (1995).

[32] Clarke, A. D., S. R. Owens, and J. Zhou. An ultrafine sea-salt flux from breaking waves: Implications for cloud condensation nuclei in the remote marine atmosphere, *J. Geophys. Res*., **111**, D06202 (2006).

[33] Wood, R., The rate of loss of cloud droplets by coalescence in warm clouds. *J.Geophys. Res*., **111**, D21205 (2006).

[34] Wood, R., M. Köhler, R. Bennartz, C. O'Dell. The diurnal cycle of surface divergence over the global oceans. *Quart. J. Roy. Meteorol. Soc*., **135,** 1484-1493 (2009).

[35] Wood, R., and C.S. Bretherton. Boundary layer depth, entrainment and decoupling in the cloud-capped subtropical and tropical marine boundary layer. *J. Clim.* 17, 3576–3588 (2004).

[36] Stevens, B. Entrainment in stratocumulus-topped mixed layers. *Quarterly Journal of the Royal Meteorological Society* **128**, 2663–2690 (2002).

[37] Wood, R. et al. The VAMOS Ocean-Cloud-Atmosphere-Land Study Regional Experiment (VOCALS-REx): goals, platforms, and field operations, *Atmos. Chem. Phys*., **11**, 627-654 (2011).

[38] Allen, G., Coe, H., Clarke, A., Bretherton, C., Wood, R., Abel, S. J., Barrett, P., Brown, P., George, R., Freitag, S., McNaughton, C., Howell, S., Shank, L., Kapustin, V., Brekhovskikh, V., Kleinman, L., Lee, Y.-N., Springston, S., Toniazzo, T., Krejci, R., Fochesatto, J., Shaw, G., Krecl, P., Brooks, B., McMeeking, G., Bower, K. N., Williams, P. I., Crosier, J., Crawford, I., Connolly, P., Allan, J. D., Covert, D., Bandy, A. R., Russell, L. M., Trembath, J., Bart, M., McQuaid, J. B., Wang, J., and Chand, D.: South East Pacific atmospheric composition and variability sampled along 20° S during VOCALS-REx, Atmos. Chem. Phys., 11, 5237-5262, doi:10.5194/acp-11-5237-2011 (2011).

[39] Feingold, G., S. M. Kreidenweis, B. Stevens, and W. R. Cotton. Numerical simulations of stratocumulus processing of cloud condensation nuclei through collision-coalescence, J. Geophys. Res., 101, 21,391–21,402 (1996).

[40] Bretherton, C. S., Wood, R., George, R. C., Leon, D., Allen, G., and Zheng, X.: Southeast Pacific stratocumulus clouds, precipitation and boundary layer structure sampled along 20°S during VOCALS-REx, *Atmos. Chem. Phys*., **10**, 10639-10654 (2010).

[41] Wood, R., C. S. Bretherton, and D. L. Hartmann. Diurnal cycle of liquid water path over the subtropical and tropical oceans. *Geophys. Res. Lett.* **10**.1029/2002GL015371 (2002).

[42] de Leeuw, G., E. L Andreas, M. D. Anguelova, C. W. Fairall, E. R. Lewis, C. O'Dowd, M. Schulz, and S. E. Schwartz: Production flux of sea spray aerosol, *Rev. Geophys*., **49**, RG2001 (2011).

[43] Clarke, A. and Kapustin, V.: Hemispheric aerosol vertical profiles: anthropogenic impacts on optical depth and cloud nuclei, *Science*, **329**, 1488–1492, (2010)

[44] Stevens, B., and G. Feingold. Untangling aerosol effects on clouds and precipitation in a buffered system. *Nature*, **461**, doi:10.1038/nature08281 (2009).

[45] Snider, J. R., S. Guibert, J. L. Brenguier, and J. P. Putaud. Aerosol activation in marine stratocumulus clouds: 2. Kohler and parcel theory closure studies. *J. Geophys. Res.*, **108**, 8629 (2003).

[46] Giorgi, F. Dry deposition velocities of atmospheric aerosols as inferred by applying a particle dry deposition parameterization to a general circulation model. *Tellus B*, **40B**, 23-41 (1988).

[47] George, R. C. and Wood, R. Subseasonal variability of low cloud radiative properties over the southeast Pacific Ocean, *Atmos. Chem. Phys*., **10**, 4047-4063, doi:10.5194/acp-10-4047-2010 (2010).

[48] Bennartz, R. Global assessment of marine boundary layer cloud droplet number concentration from satellite, J. Geophys. Res., 112, D02201 (2007).

[49] Lebsock, M. D., and T. S. L'Ecuyer, The retrieval of warm rain from CloudSat, *J. Geophys. Res*., doi:10.1029/2011JD016076 (2011).

Acknowledgements:

The authors would like to thank the staff and crew of the NSF/NCAR C-130 aircraft whose dedication resulted in the in-situ observational VOCALS Regional Experiment dataset. The CloudSat data were distributed by the CloudSat Data Processing Center at Colorado State University. MODIS data were obtained from the NASA Goddard Land Processes data archive. QuikScat data were produced by Remote Sensing Systems and sponsored by the NASA Ocean Vector Winds Science Team. This work was supported by NASA award numbers NNX10AN78G and NNX10AM29G and NSF award numbers ATM-0745702 and ATM-0745368.

Author contributions:

RW conducted the bulk of the observational analysis and model results, provided the overall synthesis and wrote the manuscript. DL provided aircraft-based precipitation estimates from the VOCALS Regional Experiment. ML provided new precipitation retrievals for low clouds using CloudSat data. JS provided the CCN measurements. ADC provided other aerosol measurements and guidance on free tropospheric aerosol variability.

Competing financial interests statement:

I declare that the authors have no competing interests as defined by Nature Publishing Group, or other interests that might be perceived to influence the results and/or discussion reported in this article.

Robert Wood

Figure legends

Figure 1: Model inputs and results from southeastern Pacific stratocumulus region from 70-90°W along 20°S. (a) Free-tropospheric (FT) aerosol concentrations (left axis) showing range of mean CCN concentrations corresponding to supersaturations relevant for cloud formation (gray shading), and total non-volatile particle concentration (open circles). Green bar shows estimated CCN for 0.2-0.5% supersaturation from measurements of FT aerosol size distributions during subsiding conditions on Mauna Loa, Hawaii, see the Methods section; cloud base precipitation rates (right axis) estimated from CloudSat satellite (mean for October/November 2006-2009 between 22°S and 18°S, red shading showing 1:30am and 1:30pm local time overpasses) and from the VOCALS-REx field experiment (black and blue squares from aircraft radar and in-situ precipitation probes respectively, in the latitude range 18-22°S); **(b)** observed (solid circles: aircraft during VOCALS[38,41], diamonds: satellite estimates from MODIS, 18-22°S) and modeled mean cloud droplet concentration N_d for different model scenarios as denoted in legend and discussed in the text.

Figure 2: Cloud droplet concentrations in regions of extensive marine low clouds observed by satellite and from the budget model. Annual mean cloud droplet concentration N_d for extensive marine low clouds under conditions of large scale subsidence, (a) from MODIS (see Methods section); (b) from the CCN budget model for the same regions.

Figure 3: Mean precipitation rate at cloud base from low clouds (cloud top height z_{top}<3 km) estimated with spaceborne radar measurements from CloudSat[49]. Data are screened to display regions of extensive marine low clouds under conditions of mean subsidence as in Fig. 2.

Figure 4: Frequency distributions of observed and modeled monthly mean cloud droplet concentration. Only months that meet the criteria needed to contribute to the means shown in Fig. 2 (regions with extensive low clouds under divergent conditions) are shown. Shown here are the base version of the model (i.e. that used to construct Fig. 2, solid black), together with estimates with no FT contribution to CCN (dashed), and no sea salt contribution (dotted). Error bars show the 95% confidence interval in the frequency estimates for the observations and for the model base case due to sampling limitations.

Table 1: The effects on the mean cloud droplet concentration in various geographical regions of changing the primary source and sink terms

Observed or model estimate	Mean cloud droplet concentration [cm^{-3}]		
	35°S-35°N	35°S-35°N within 300 km of coastlines	60°S-60°N
Observations (MODIS)	**88**	**152**	**74**
Model, base case (N_{FT} = 125 cm^{-3})	88	129	74
Model, N_{FT} = 0	20	21	25
Model, no SSA	68	109	46
Model, no precipitation	169	150	245
Model, N_{FT} = 80 cm^{-3}	63	90	55
Model, N_{FT} = 160 cm^{-3}	107	154	85

Table 2: Geographical variability of cloud droplet concentration for various model configurations. Results show correlation coefficients between annual mean MODIS observed and model estimates of annual mean N_d and the ratio of the model and observed standard deviations ($\sigma_{model}/\sigma_{obs}$). Correlations not significant at the 2σ level are italicized. All results are for the tropics and subtropics (35°S-35°N).

Model configuration	r (obs, model)	$\sigma_{model}/\sigma_{obs}$
Base case	0.65	0.92
P_{CB} variability only	0.77	1.01
P_{CB} and U_{10} variability only	0.70	0.97
U_{10} variability only	*-0.06*	0.37
D variability only	0.21	0.18
h variability only	0.37	0.13
z_i variability only	-0.32	0.10

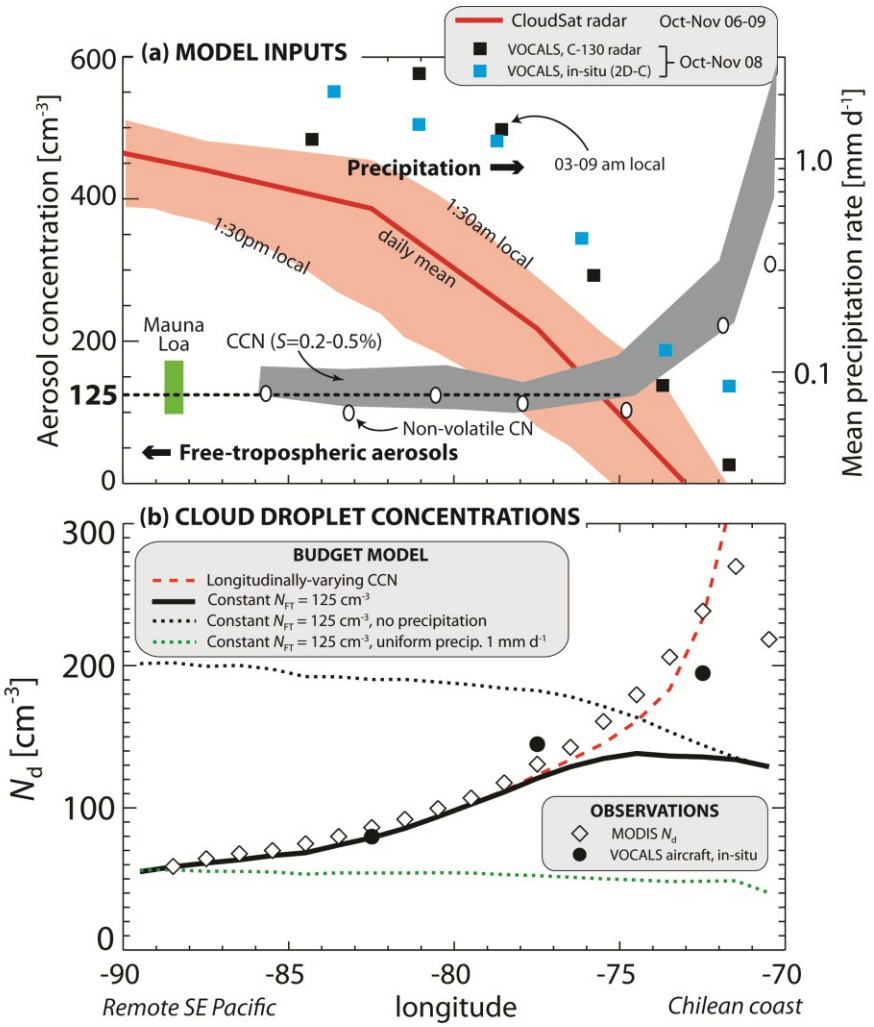

Figure 1: Model inputs and results from southeastern Pacific stratocumulus region from 70-90°W along 20°S. (a) Free-tropospheric (FT) aerosol concentrations (left axis) showing range of mean CCN concentrations corresponding to supersaturations relevant for cloud formation (gray shading), and total non-volatile particle concentration (open circles). Green bar shows estimated CCN for 0.2-0.5% supersaturation from measurements of FT aerosol size distributions during subsiding conditions on Mauna Loa, Hawaii, see the Methods section; cloud base precipitation rates (right axis) estimated from CloudSat satellite (mean for October/November 2006-2009 between 22°S and 18°S, red shading showing 1:30am and 1:30pm local time overpasses) and from the VOCALS-REx field experiment (black and blue squares from aircraft radar and in-situ precipitation probes respectively, in the latitude range 18-22°S); **(b)** observed (solid circles: aircraft during VOCALS[38,41], diamonds: satellite estimates from MODIS, 18-22°S) and modeled mean cloud droplet concentration N_d for different model scenarios as denoted in legend and discussed in the text.

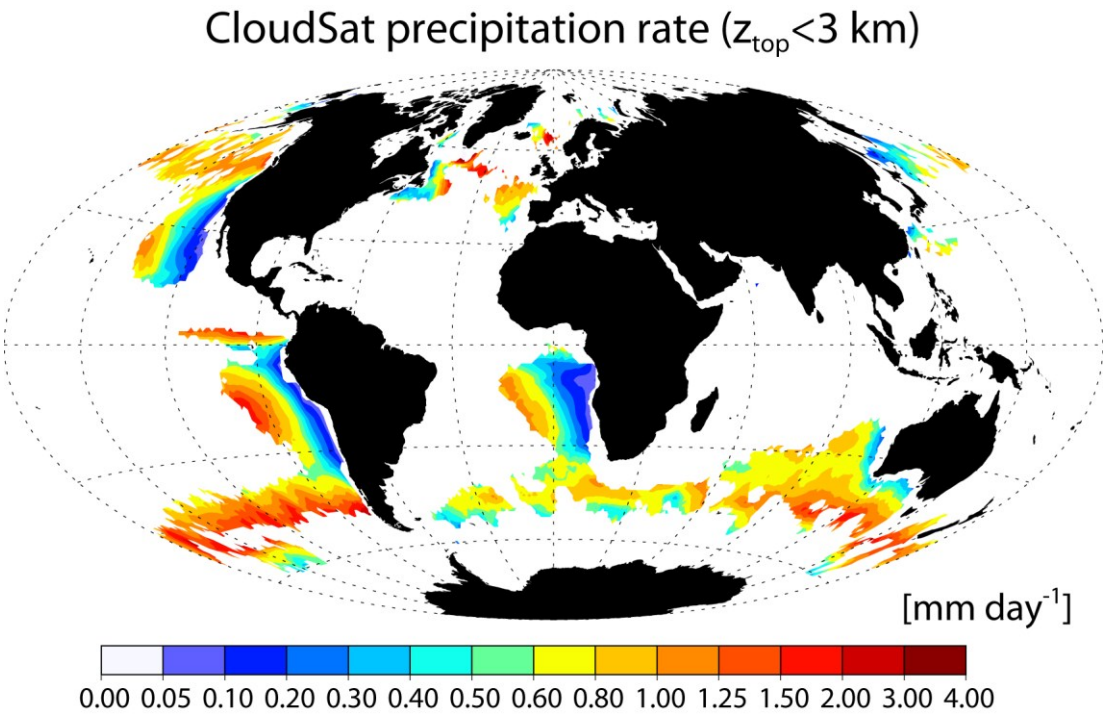

Figure 2: Cloud droplet concentrations in regions of extensive marine low clouds observed by satellite and from the budget model. Annual mean cloud droplet concentration N_d for extensive marine low clouds under conditions of large scale subsidence, (a) from MODIS (see Methods section); (b) from the CCN budget model for the same regions.

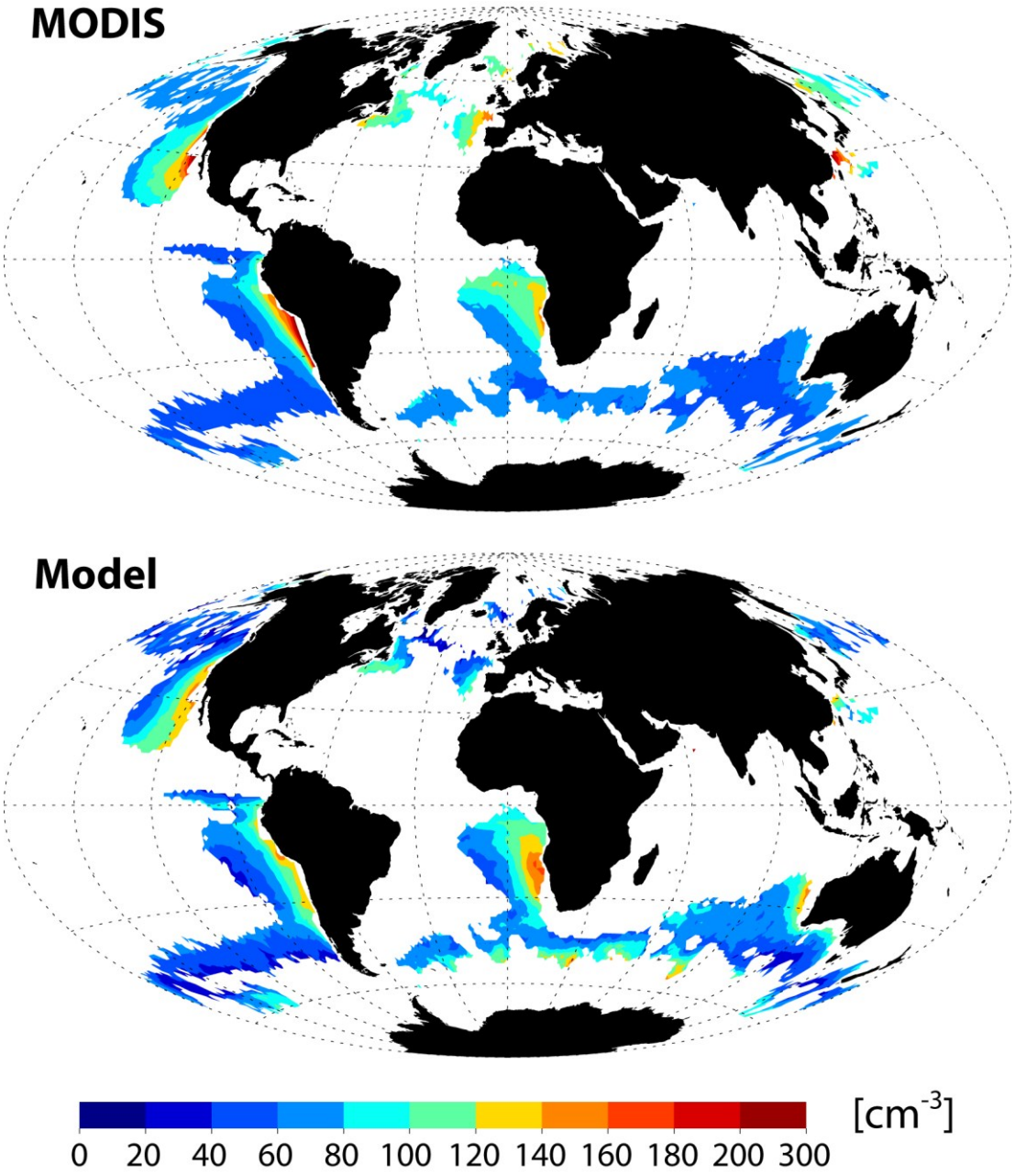

Figure 3: Mean precipitation rate at cloud base from low clouds (cloud top height z_{top}<3 km) estimated with spaceborne radar measurements from CloudSat[49]. Data are screened to display regions of extensive marine low clouds under conditions of mean subsidence as in Fig. 2.

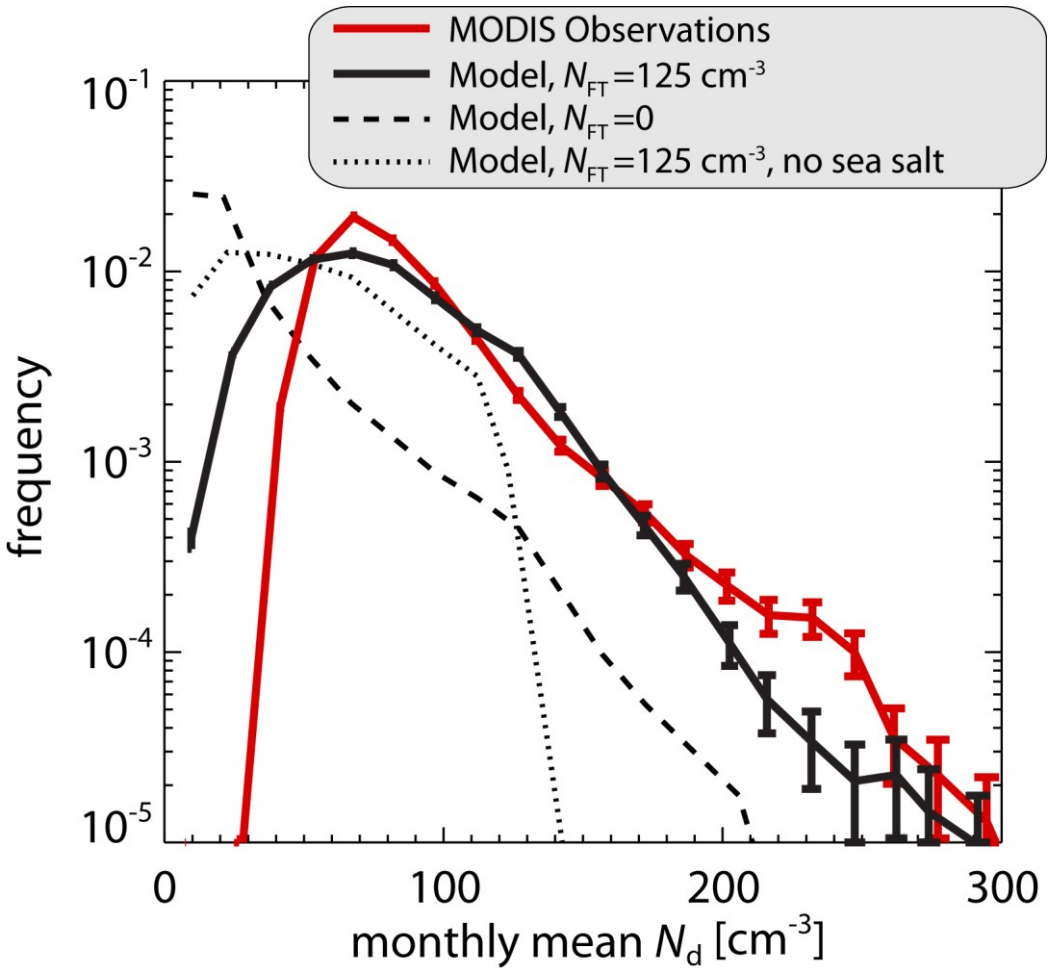

Figure 4: Frequency distributions of observed and modeled monthly mean cloud droplet concentration. Only months that meet the criteria needed to contribute to the means shown in Fig. 2 (regions with extensive low clouds under divergent conditions) are shown. Shown here are the base version of the model (i.e. that used to construct Fig. 2, solid black), together with estimates with no FT contribution to CCN (dashed), and no sea salt contribution (dotted). Error bars show the 95% confidence interval in the frequency estimates for the observations and for the model base case due to sampling limitations.

SUPPLEMENTARY INFORMATION

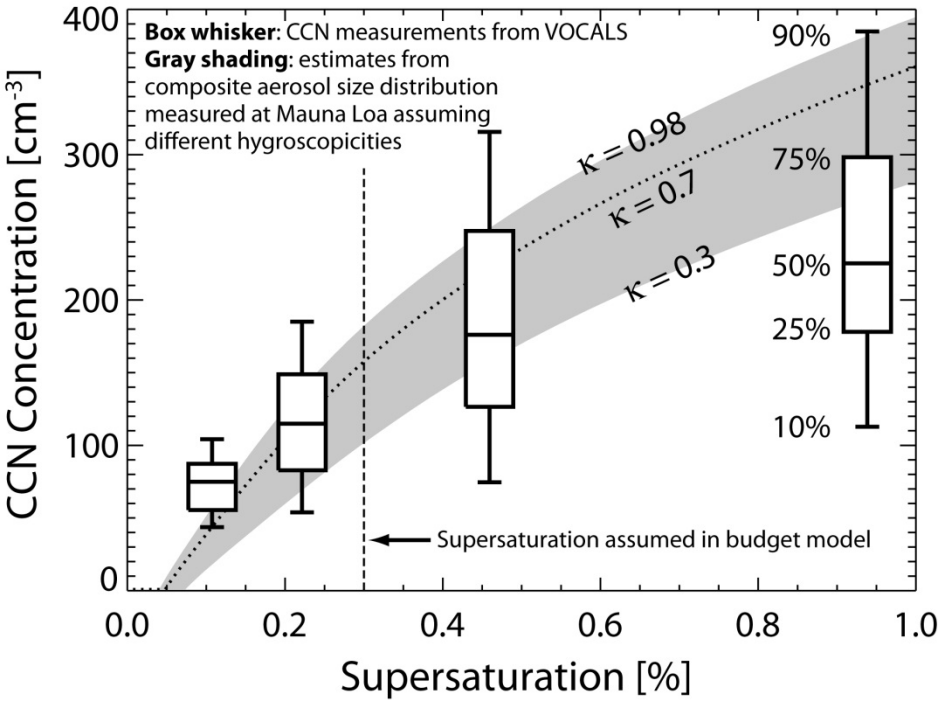

Supplementary Figure 1: Free-tropospheric CCN spectra from the southeastern Pacific and Hawaii. Observations from the southeastern Pacific are from CCN spectra taken in the remote FT west of 75°W using the NSF/NCAR C-130 aircraft in VOCALS[39,40], corrected to an assumed mean MBL pressure of 925 hPa. Box-whisker plots show the 10th, 25th, 50th , 75th, and 90th percentile concentrations for four supersaturations from 638 CCN measurements (61, 117, 147 and 313 at supersaturations of approximately 0.1, 0.25, 0.5 and 0.9% respectively) over the month-long campaign. Details of the CCN measurements are provided in Snider et al. (2006). Shaded region shows a plausible range of CCN concentration estimated using the composite size distribution for subsiding FT air measured on Mauna Loa in Hawaii[31], corrected to an assumed mean MBL pressure of 925 hPa, with the spread representing a plausible range of hygroscopicity κ parameters (Petters and Kreidenweis 2007) for clean FT air. The lower boundary (κ=0.3) is approximately the lowest value of CCN-based hygroscopicity measured in the FT from Roberts et al. (2010). The upper boundary (κ=0.98) is the geometric mean value from Roberts et al. (2010). Values of κ significantly higher than 1 were inferred from CCN measurements in Roberts et al. (2010) but seem implausible given that even the most hygroscopic compounds have κ values of about unity (Petters and Kreidenweis 2007). Ammonium sulfate has a κ value of approximately 0.7 (Petters and Kreidenweis 2007) and is shown by the dotted line.

The peak supersaturation σ = 0.3% assumed in the model is assumed to be constant everywhere. Understanding how this changes systematically over the remote oceans is complex, as it depends upon variations in the strength of the turbulent updrafts and upon the size distribution of the aerosol being activated[4,46]. We use recent field measurements of mean aerosol size distributions at different distances from the Chilean coast from the VOCALS Regional Experiment[38] to estimate the likely systematic geographical variability in σ. In the marine boundary layer, the

Hoppel minimum (Hoppel 1986) in the size distribution is indicative of the minimum size of aerosols that are activated. Assuming a hygroscopic aerosol, this minimum size is directly related to the supersaturation. A systematic reduction from 0.1 to 0.07 μm in the minimum diameter was observed to occur from 70°W to 78°W moving westwards along 20°S away from the Chilean coast (Kleinmann et al. 2012). This implies that the mean supersaturation increases by ~75% from the coast offshore. However, the coastal CCN concentrations are high consistent with pollution aerosol impacts[39], and so these are not representative of the supersaturations we are attempting to represent in the model. No systematic shift in the Hoppel minimum is observed over the cleaner region from 74°W to 78°W, suggesting that systematic changes in supersaturation over the remoter regions may be considerably smaller than occur near the coasts.

Hoppel, W. A., Frick, G. M., and Larson, R. E.: Effects of nonprecipitating clouds on the aerosol size distribution in the marine boundary layer, Geophys. Res. Lett., 13, 125–128, 1986.

Kleinman, L. I., Daum, P. H., Lee, Y.-N., Lewis, E. R., Sedlacek III, A. J., Senum, G. I., Springston, S. R., Wang, J., Hubbe, J., Jayne, J., Min, Q., Yum, S. S., and Allen, G.: Aerosol concentration and size distribution measured below, in, and above cloud from the DOE G-1 during VOCALS-REx, Atmos. Chem. Phys., 12, 207-223, doi:10.5194/acp-12-207-2012, 2012.

Petters, M. D. and Kreidenweis, S. M.: A single parameter representation of hygroscopic growth and cloud condensation nucleus activity, Atmos. Chem. Phys., 7, 1961-1971, doi:10.5194/acp-7-1961-2007, 2007.

Roberts, G. C., Day, D. A., Russell, L. M., Dunlea, E. J., Jimenez, J. L., Tomlinson, J. M., Collins, D. R., Shinozuka, Y., and Clarke, A. D.: Characterization of particle cloud droplet activity and composition in the free troposphere and the boundary layer during INTEX-B, Atmos. Chem. Phys., 10, 6627-6644, doi:10.5194/acp-10-6627-2010, 2010.

Snider, J. R., M. D. Petters, P. Wechsler and P. Liu, Supersaturation in the Wyoming CCN instrument, *J. Atmos. Oceanic Technol.*, 23, 1323-1339, 2006.

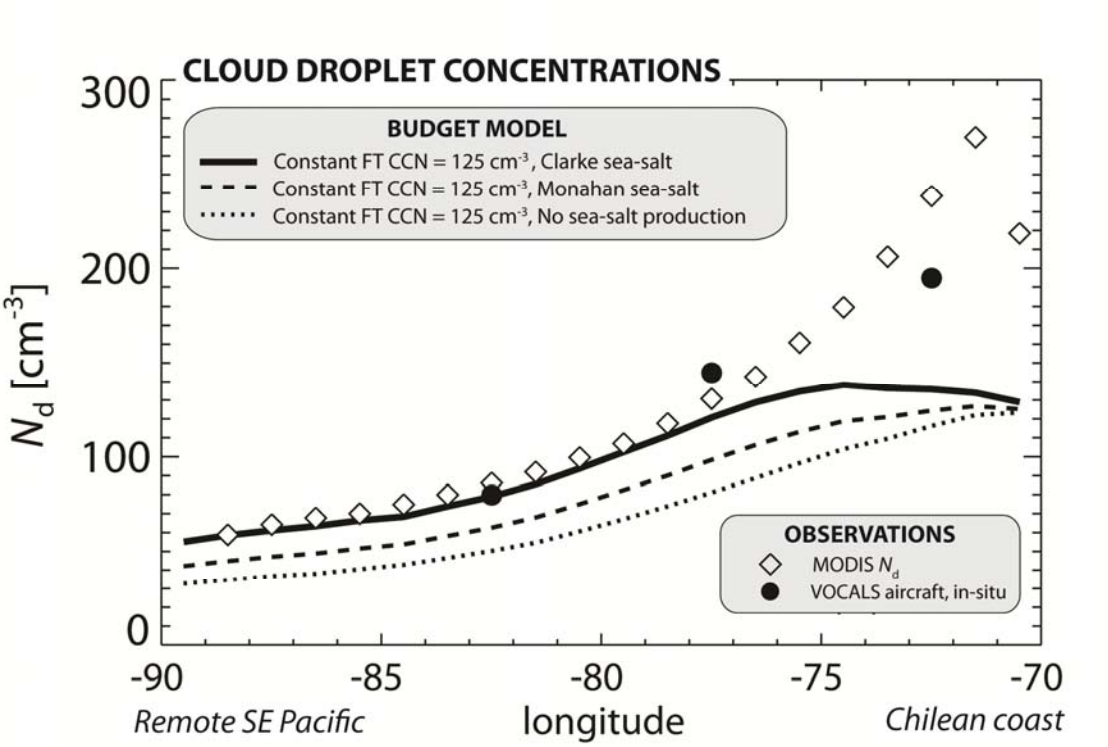

Supplementary Figure 2: Effects of different assumptions regarding primary production of sea-salt in the model. Same as Figure 1 in the manuscript, but showing sensitivity to sea-salt aerosol parameterization used. Observed (solid circles: aircraft during VOCALS[39,42], diamonds: satellite estimates from MODIS, 18-22°S) and modeled mean cloud droplet concentration N_d. Solid line: standard model set up with constant FT CCN. Dashed line: Monahan sea-salt parameterization (Monahan et al. 1986) in place of the Clarke[34] parameterization. Dotted line: No primary production of sea-salt at all. The concentration of CCN from sea-salt (the difference between the solid and the dotted line) ranges from <10 cm^{-3} close to the Chilean coast, where wind speeds are low, to around 40 cm^{-3} further afield, where wind speeds are higher. These findings are consistent with preliminary measurements from aircraft during VOCALS (Anthony Clarke, personal communication).

Monahan, E. C., D. E. Spiel, and K. L. Davidson (1986), A model of marine aerosol generation via whitecaps and wave disruption, in Oceanic Whitecaps and Their Role in Air-Sea Exchange Processes, edited by E. C. Monahan and G. Mac Niocaill, pp. 167– 193, Springer, New York.

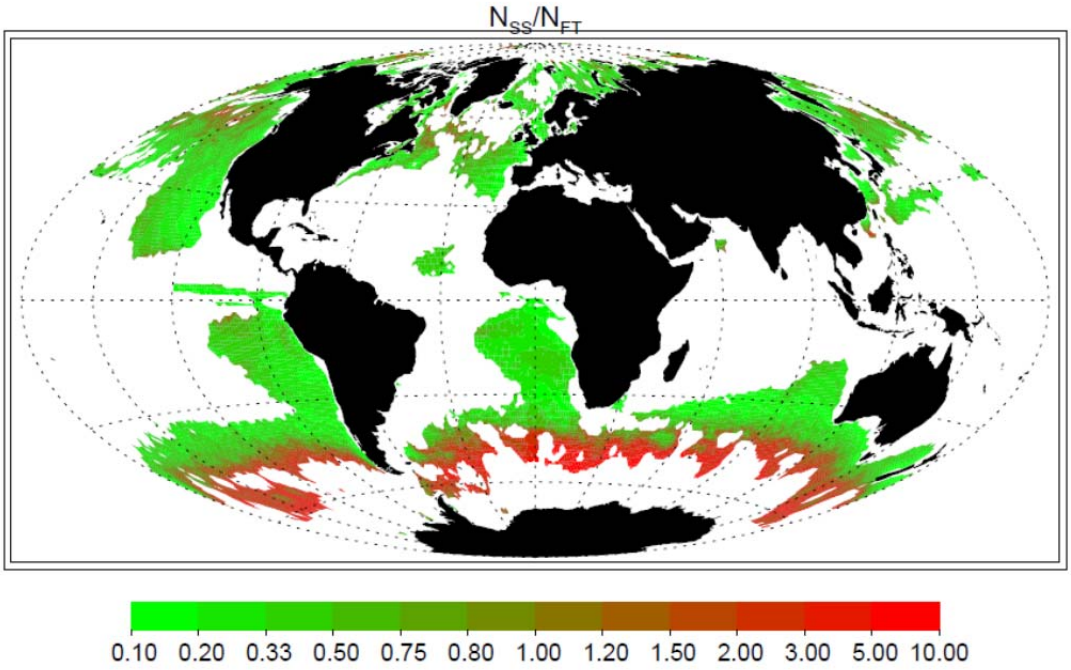

Supplementary Figure 3: Ratio of CCN flux from surface to that from entrainment from the free troposphere (FT) in the model. The FT CCN concentration is set to 125 cm^{-3} and the surface source depends upon daily wind speed. In the subtropics and tropics, the majority of the CCN originate from the FT, but in the midlatitudes where winds are stronger, the surface source can exceed that from the FT.

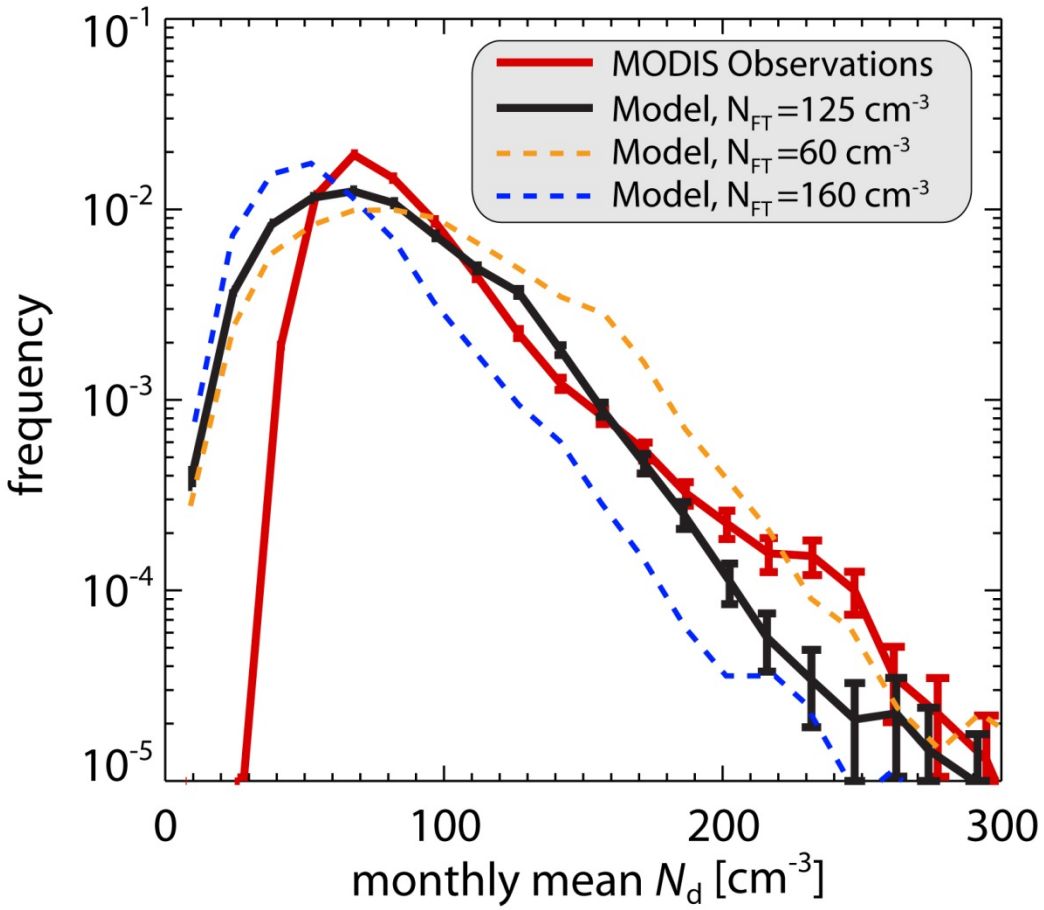

Supplementary Figure 4: Sensitivity to assumed free tropospheric CCN concentration N_{FT} of the frequency distributions modeled monthly mean cloud droplet concentration. Only months that meet the criteria needed to contribute to the means shown in Fig. 2 (regions with extensive low clouds under divergent conditions) are shown. Shown here are the base version of the model (i.e. that used to construct Fig. 2, solid black), together with model estimates with low (N_{FT} = 80 cm^{-3}) and high (N_{FT} = 160 cm^{-3}) estimates of the FT contribution to CCN (dashed blue and orange respectively). Error bars show the 95% confidence interval in the frequency estimates for the observations and for the model base case due to sampling limitations.